Optoelectronic Bidirectional Transceiver Chips: Crosstalk and Alignment Issues

Alexander Kern

We present the static operation properties of monolithically integrated 850 nm wavelength AlGaAs/GaAs-based vertical-cavity surface-emitting lasers (VCSELs) and PIN (p-doped–intrinsic–n-doped) photodiodes (PDs). Devices with three different epitaxial layer structures of the PDs are investigated. PDs with a 3 µm thick intrinsic region show a responsivity of $> 0.6\,A/W$ and have the lowest dark currents. We investigate the mutual influence between the closely integrated optoelectronic devices. The optical crosstalk is below -11 dB and the maximum electrical crosstalk between VCSEL and PIN PD of around -50 dB is nearly negligible. Butt-coupling to a multimode fiber with a core diameter of 50 µm has maximum fiber alignment tolerances in the range of 14–26 µm.

1. Introduction

For some years we have been doing research into novel transceiver (TRx) devices which integrate VCSELs and PIN PDs for operation in the standard wavelength regime at around 850 nm wavelength. The stacked layer structure requires sophisticated fabrication methods but enables the use in bidirectional short-reach optical data links over a single butt-coupled standard multimode fiber (MMF). Chip fabrication is described in [1] in some detail. As can be seen in Fig. 1, all transceiver device contacts with ground–signal–ground configuration are accessible from the top by two coplanar microwave probes for PD and VCSEL. Thus, static and high-speed operation of the devices is enabled on-wafer without the need for chip separation.

Recently we have reported error-free (bit error ratio $< 10^{-12}$) data transmission experiments (1) at 7 Gbit/s (half-duplex) and 6 Gbit/s (full-duplex) over 500 m of an OM3-type MMF [2], (2) at 8 Gbit/s (full-duplex) in back-to-back operation [1], and (3) at 11 Gbit/s (half-duplex) and 10 Gbit/s (full-duplex) over 550 m OM4 MMF and even at 12.5 Gbit/s (full-duplex) back-to-back [3]. In this report we focus on the static operation characteristics of latest-generation TRx chips and investigate electrical and optical crosstalk as well as the alignment tolerances for butt-coupling to a 50 µm core diameter MMF.

2. Static Device Characteristics

2.1 Transceiver VCSEL

The miniaturized integrated VCSEL with a mesa diameter of 25 µm has an oxide-confined current aperture of 6.4 µm for multimode operation. Figure 2 shows the output characteristics of such a top-emitting device for four different ambient temperatures. The threshold

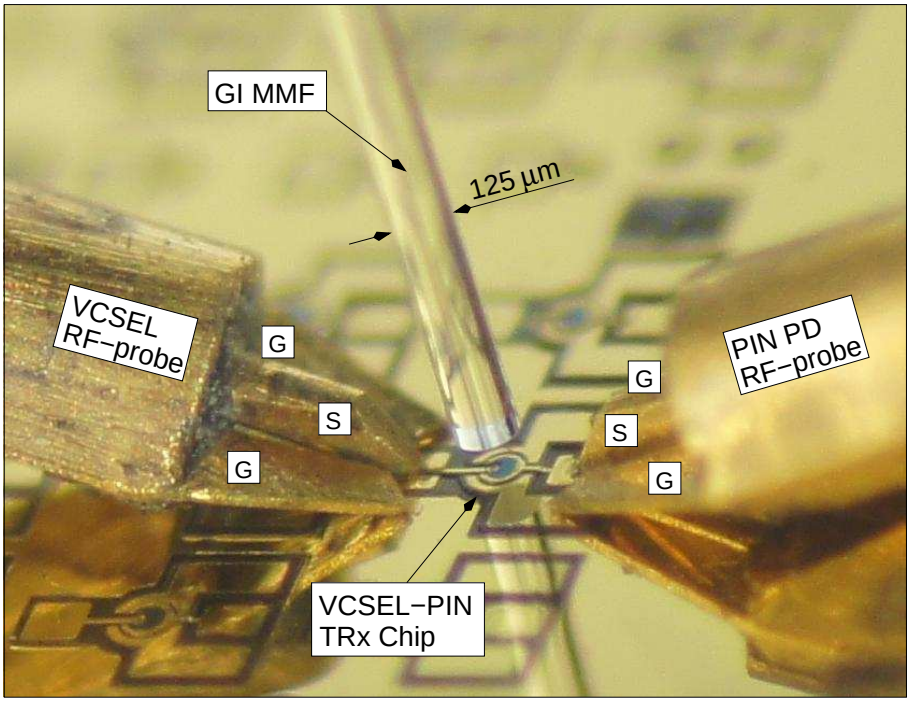

Fig. 1: Photograph of an on-wafer tested VCSEL–PIN transceiver chip butt-coupled to a standard MMF. The TRx chip is contacted with two ground–signal–ground (GSG) microwave probes for high-speed operation.

current is 1.2 mA, the maximum output power at thermal rollover is 4.5 mW at 12 mA injection current, and the slope efficiency amounts to 0.51 W/A at 5.9 mA bias current and room temperature. Taking the emission wavelength of around 823 nm at the same bias current and ambient temperature into account (see the inset in Fig. 2), a relatively low differential quantum efficiency of around 34 % is obtained. The short emission wavelength of the VCSEL originates from a VCSEL position far away from the center of the wafer, where the layers are thinner due to inhomogeneous growth by molecular beam epitaxy (MBE). As can be seen from the continuous increase of the threshold current with temperature, the cavity modes have shorter wavelengths than the gain peak even at room temperature. In other words, the VCSEL has negative detuning. In an improved device generation, positive detuning should be chosen, which will benefit the high-temperature characteristics of the device. A red-shift of the emission wavelength of around 4 nm in the inset of Fig. 2 occurs over 60 °C temperature increase, which corresponds to a well-known wavelength shift of approximately 0.065 nm/K induced by the refractive index change of the AlGaAs/GaAs materials [4]. At the same time, the threshold of the VCSEL increases by 1 mA and the maximum output power at rollover drops by 2.5 mW. Also the differential quantum efficiency at 80 °C drops to 20 % at 5.9 mA. The differential resistance extracted by linear interpolation of the current–voltage curve at high operating currents is 116 Ω and is almost constant with temperature.

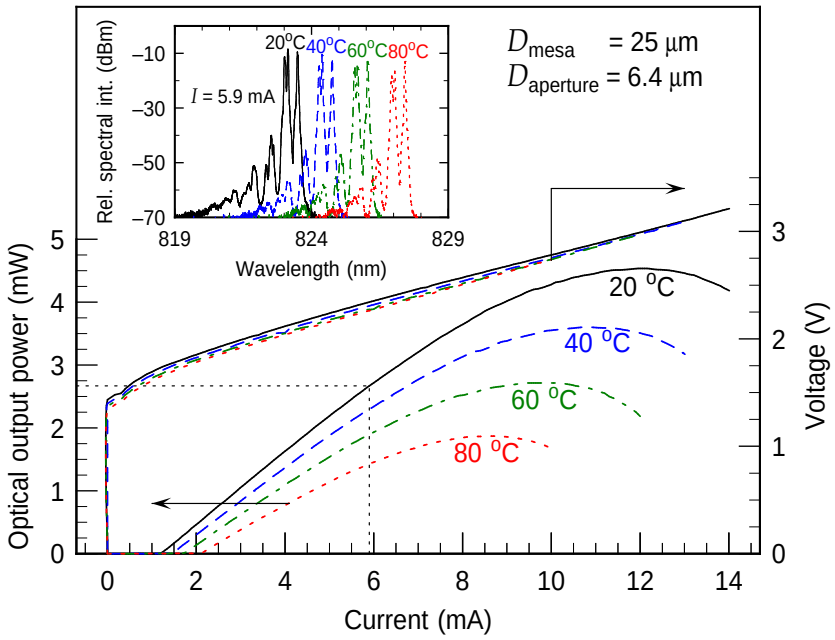

Fig. 2: Continuous-wave light–current–voltage characteristics of a TRx VCSEL for different ambient temperatures. The inset shows multimode emission spectra at a laser current of $I = 5.9\,\mathrm{mA}$ with a characteristic shift towards longer wavelengths for higher temperatures.

2.2 Transceiver PIN photodiode

For evaluation purposes, three different samples were grown, containing an identical epitaxial VCSEL structure but 1, 2, and 3 µm thick i-GaAs absorption regions of the PIN photodiode. Due to different chip topographies of up to several micrometers, more polyimide planarization steps had to be applied for thicker PDs. All three transceiver samples were anti-reflection-coated with a quarter-wave Al_2O_3 layer for 850 nm incident light, thus reducing the reflectivity at the semiconductor surface from initially approximately 30 % to 1.3 % over a spectral width of nearly 50 nm [5]. After the first transmission through the i-GaAs, the VCSEL structure underneath the photodetector leads to back-reflection of the non-absorbed portion of the incident light and thus to double-pass absorption. The increase of the responsivity and quantum efficiency for 1 µm thick PDs was reported in [6]. As can be seen in Fig. 3, the measured responsivity of a PIN photodiode with 2 µm thick absorption region is 0.66 A/W for an incident wavelength of $\lambda = 858\,\mathrm{nm}$ and thus nearly 16 % higher compared to a 1 µm PD with 0.57 A/W. This corresponds to 95 % and 82 % quantum efficiency, respectively. Unfortunately, the responsivity of the photodiode with 3 µm thick GaAs absorption layer is only 0.62 A/W, which corresponds to a quantum efficiency of 90 %. The relatively low value arises from the detuned VCSEL structure for the given sample. The reflectivity of the underlying DBR pair is only about 40 % at the measured incident light wavelength of 858 nm. Therefore only a reduced portion of the reflected light can be absorbed in the PD. Taking an absorption coefficient of $9000\,\mathrm{cm}^{-1}$ for high-purity GaAs at around 850 nm [7] and ideal reflection of the VCSEL stop-band into account, a maximum responsivity of 0.68 A/W and thus a quantum efficiency of 98 % is theoretically achievable for a 3 µm thick PIN PD.

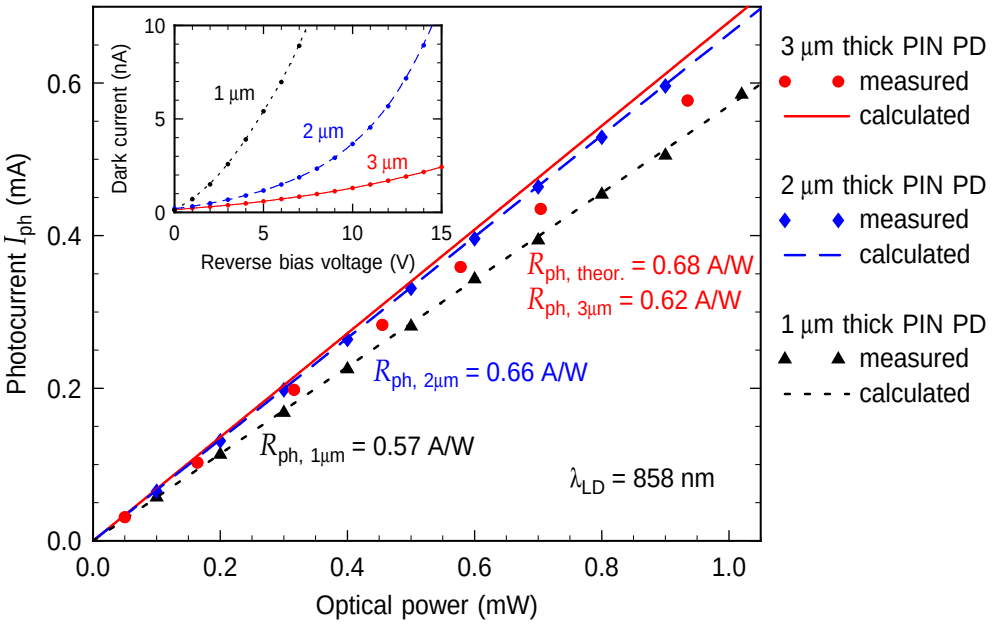

Fig. 3: Comparison of the measured (symbols) and calculated (lines) responsivities of integrated transceiver PIN PDs for samples with 1, 2, and 3 µm thick absorption regions for a laser emission wavelength of 858 nm. The inset shows the dark current behavior of PIN devices with different thicknesses for the reverse bias voltage range from 0 to 15 V.

The inset in Fig. 3 shows the dark current dependence of the three different PIN PDs with respect to the applied reverse bias voltage. Comparing the dark currents for identical values of the electric field strength in the absorption region, i.e., 3 V for 1 µm, 6 V for 2 µm, and 9 V for 3 µm thick PDs, it is < 2 nA for all photodetectors. The main reason for the exponential growth of the dark current is the increasing tunneling probability of the carriers due to stronger band bending for higher reverse bias voltages [4]. For optical data transmission experiments, the noise attributed to dark current can be neglected within the range of applied operating voltages.

3. Crosstalk Behavior of the Transceiver Chips

In this section we investigate the electrical and optical crosstalk in the closely integrated devices, which is important for full-duplex operation.

3.1 Electrical crosstalk

After the separate electro–optical as well as purely electrical characterization of the transmitter (Tx) and receiver (Rx), it is also necessary to investigate the mutual influence of the VCSEL and PIN PD, leading to a higher noise level in full-duplex mode operation of the transceiver chip. Owing to the very dense monolithic integration of the Tx and Rx, one might expect that a portion of the electrical power is coupled from the VCSEL

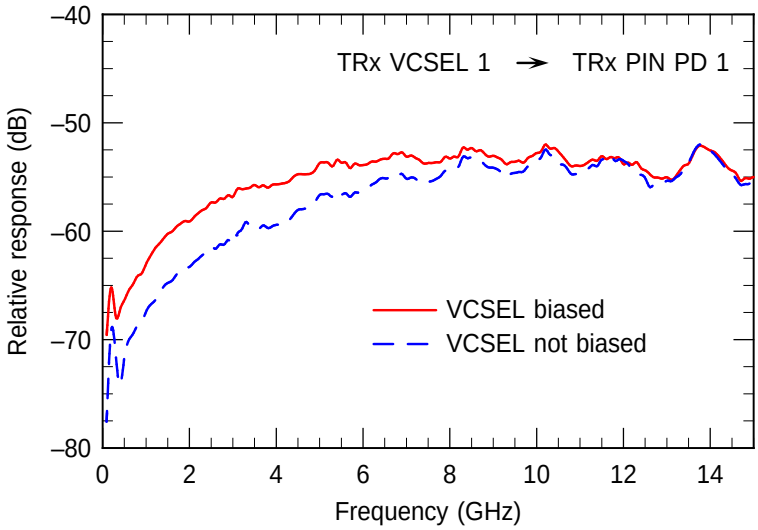

Fig. 4: Small-signal frequency response curves of electrically induced crosstalk between a VCSEL and a PIN PD of the same transceiver chip.

to the photodetector. In the experiment, a solitary TRx chip was contacted by two microwave probes as in Fig. 1, however, without the fiber in place. The VCSEL is driven by a low-power modulating signal generated by a sweep oscillator. On the PD side, the coupled electrical power is measured by an electrical spectrum analyzer. Figure 4 shows the frequency responses as ratios of both signals for a biased and unbiased state of the VCSEL. Both curves indicate a high-pass characteristic starting from around −70 dB coupling for MHz frequencies and increasing to values still well below −50 dB for frequencies between 8 and 15 GHz. Thus, the contribution to the system noise originating from electrical crosstalk is negligible. Nevertheless, at lower frequencies, the crosstalk for a biased VCSEL is up to 5 dB higher compared to VCSEL operation below threshold. The higher values can be attributed to optical crosstalk between VCSEL and PIN PD, where a small portion of the emitted light is directly detected by the photodetector. This is discussed in more detail in the following subsection. As expected, the difference vanishes for high frequencies above the bandwidth of the PD.

3.2 Optical crosstalk

Although VCSEL and PIN PD are densely integrated, both devices are electrically isolated by a narrow, deep trench. Therefore the electrical crosstalk was expected to be very low. However, optical crosstalk can also lead to a bandwidth trade-off in full-duplex mode operation. Inspecting the schematic of a MMF butt-coupled TRx link in Fig. 5, we can identify two main sources of optical crosstalk, namely the reflections of the emitted light at the near and far ends of the fiber as well as at the opposite TRx chip. Additionally, as already mentioned in the previous subsection, there is direct light detection by the integrated photodetector. In Fig. 6, the amount of static optical crosstalk is presented as a function of the optical power of one of the VCSELs. The measurements were performed in the transmission direction from chip 2 to chip 1. We thus detect the optical crosstalk of

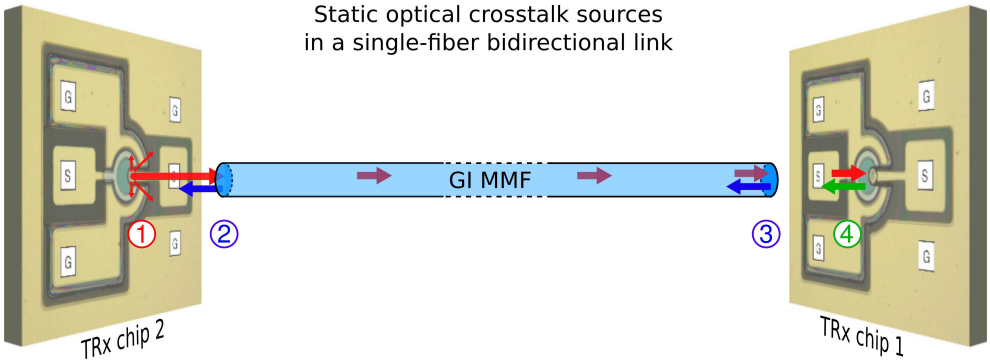

Fig. 5: Schematic illustrating the four origins of optical crosstalk for chip 2 in half-duplex operation of a data link from chip 2 to chip 1.

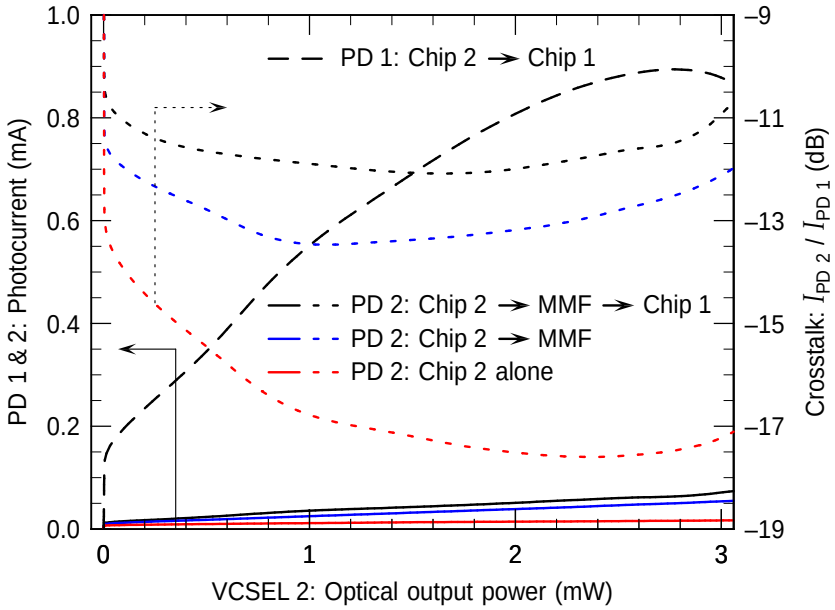

Fig. 6: Static optical crosstalk sources for chip 2 (solid and dotted) compared to the transmitted signal power to chip 1 (dashed) in a butt-coupled single-fiber bidirectional transceiver link.

PD 2 originating from VCSEL 2. For comparison, the transmitted signal power detected by PD 1 is plotted as black dashed line. Its slope decreases with higher laser power. The probable underlying reason is the changing beam profile and thus lower fiber coupling efficiency of the multimode VCSEL with higher laser current.

In the first step, similar to the measurement of electrical crosstalk in the previous subsection, the solitary TRx chip 2 was operated. Here, only direct current (DC) but no modulation was applied to VCSEL 2. The optical crosstalk then arises from the spontaneous emission of the VCSEL. Carrier clamping prevents a significant increase of photocurrent 2 (red solid line) for higher output powers. The red dotted line in Fig. 6 refers to the vertical axis on the right and quantifies the amount of optical crosstalk over the received optical power at the opposite PD 1. Here, for the common operating regime of VCSEL 2, it is about 17 dB below the signal power and thus nearly negligible.

In the second step, a 5 m long MMF was butt-coupled (about 30 µm distance) to TRx chip 2. The measured optical crosstalk (blue solid line) now originates additionally from the reflections at both fiber ends. In Fig. 6 (blue dotted line), the crosstalk increases by 4–5 dB.

Finally, TRx chip 1 was coupled to the other end of the MMF. The photocurrent of PD 2 (black solid line) increases by approximately another 1 dB due to the reflections at the opposite chip 1. Thus, the total amount of optical crosstalk power (black dotted line) is at least 11 dB below the transmitted signal power (black dashed line). It is important to mention that the total amount of optical crosstalk is dependent on the alignment of the MMF to the TRx chips and might vary from chip 1 to 2.

4. MMF–TRx Chip Alignment Tolerances

Due to the fact that VCSEL and PIN PD are butt-coupled to a single MMF without any use of external optics, it is essential to investigate the allowed fiber misalignment. The inherent misalignment of the VCSELs to the fiber core influences the optical crosstalk and the achievable bandwidth in both, half- and full-duplex mode.

For the measurement of the Rx detection efficiency, a VCSEL was coupled to the far end of a GI MMF with 50 µm core diameter, whereas the near end was mounted on a computer-controlled translation stage with an adjustment tolerance of < 1 µm. The coupling efficiency of the Tx was determined in the opposite way by coupling a TRx VCSEL to the moveable near end of the MMF and detecting the transmitted optical power at the far end. For the sake of simplicity, we chose the center of the VCSEL aperture in the TRx chip as the origin of a coordinate system. For both experiments, the initial position of the fiber core was at $x_0 = -18$ µm, $y_0 = 0$, as indicated by the solid circles in Fig. 7. In this position, the near end of the MMF is $z_0 = 30$ µm away from the TRx chip surface in order to prevent an etalon effect.

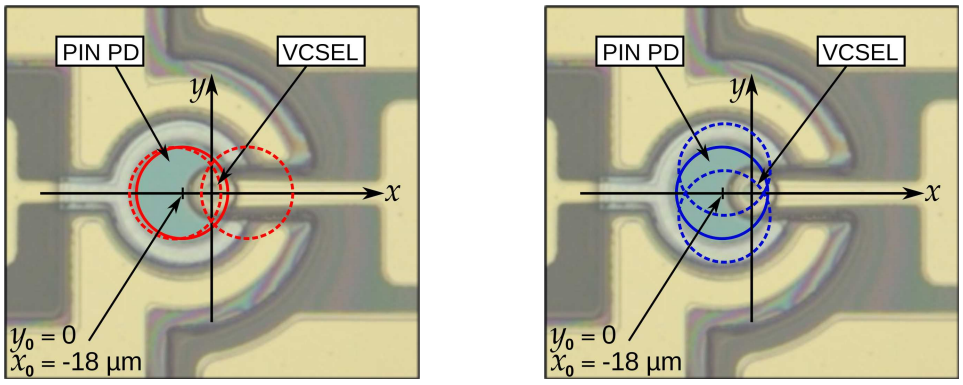

Fig. 7: Photograph of a TRx chip with positions of the 50 µm diameter fiber core for misalignments in x- (left) and y-directions (right). The dashed circles indicate the maximum possible fiber misalignment for VCSEL–fiber coupling and the solid circles show the optimum alignment at x_0 and y_0 for bidirectional data transmission experiments.

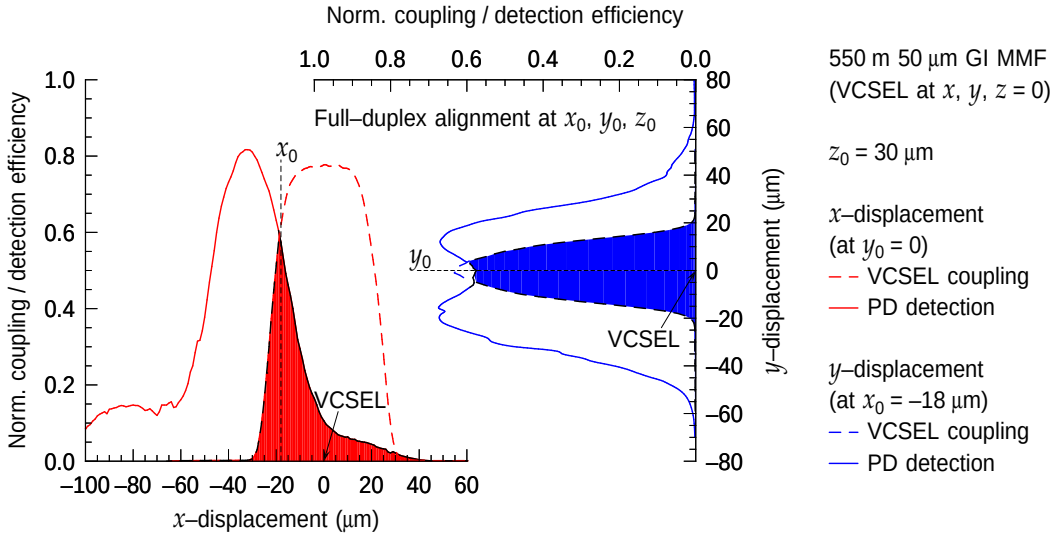

Fig. 8: Measurement of VCSEL–fiber coupling (dashed) and photodetector detection efficiency (solid) in a single-fiber bidirectional link for x- (red) and y-displacement (blue) of a butt-coupled MMF with about $z_0 = 30\,\mu\text{m}$ distance.

In the first step, the fiber was moved along the y-direction at $x_0 = -18\,\mu\text{m}$. In Fig. 8 the detection efficiency of the photodetector reaches maximum values of ~ 0.65 at $y = \pm 15\,\mu\text{m}$ (blue solid line), where the fiber core has the best overlap with the PD area. An efficiency of 1 is only possible with full-area circular photodiodes in which the photoactive area is not partly occupied by a VCSEL. A coupling efficiency of 0.6 is measured for the VCSEL at y_0, with a strong decrease when the fiber is moved away from the initial position (blue dashed line). The maximum possible y-misalignment range is indicated in Fig. 7 (right) by two blue dashed circles. Therefore in y-direction, the maximum achievable alignment tolerance is limited only by the coupling efficiency of the VCSEL as illustrated by the blue shaded area in Fig. 8. The full-width at half-maximum (FWHM) is 26 µm ($y \approx \pm 13\,\mu\text{m}$).

In the second step, the near end of the fiber was moved along the x-axis at $y_0 = 0$. Since the VCSEL is positioned 18 µm off-center in the x-direction with respect to the PD, the curves for the detection and coupling efficiencies are also displaced. Here, maximum efficiencies of ~ 0.8 can be achieved for each individual device. However, the combined maximum efficiency is ~ 0.6. Although the curve for the coupling efficiency of the VCSEL (red dashed line in Fig. 8) is wider compared to the measurement in y-direction, the allowed displacement for the PD detection (red solid line) is narrower. The overlap of both measurements, indicated by the red shaded area in Fig. 8, defines the alignment tolerance with a FWHM of 14 µm ($x \approx \pm 7\,\mu\text{m}$). Therefore misalignments in x-direction are more critical compared to the y-direction.

In summary, the optimal MMF–TRx chip alignment is a compromise between the VCSEL coupling efficiency and the PD detection efficiency. It is found at x_0, y_0 for the highest common values of the red and blue shaded areas in Fig. 8. In future, a centered (and ideally also smaller) TRx VCSEL which is surrounded by the PD would be an improvement regarding easier chip alignment, as already shown in [5] for VCSEL–MSM (metal–semiconductor–metal) TRx chips.

5. Conclusion

We have presented latest results on fully integrated 850 nm wavelength transceiver chips for single-fiber bidirectional optical data transmission. The chips consist of PIN photodiodes and oxide-confined, top-emitting VCSELs, integrated to match with butt-coupled 50 µm core diameter GI MMFs.

PIN PDs with an intrinsic absorption region thickness of 3 µm show dark currents below 2 nA and an estimated quantum efficiency of nearly 98 % for an optimum Bragg mirror design. Those PDs also have highest 3-dB bandwidths of around 8 GHz. The maximum small-signal bandwidth of the VCSEL is 12.5 GHz and thus the highest operation data rate of the transceiver chip is limited by the PIN PD. The dynamic characteristics were not reported here.

We have investigated the crosstalk properties of the integrated devices, since they affect the data transmission in full-duplex mode. The optical crosstalk is 11 dB below the signal photocurrent level and originates from the reflections at both fiber ends and at the opposite TRx chip as well as from spontaneous emission of the adjacent VCSEL. The electrical crosstalk between VCSEL and PIN PD of the same chip is attenuated by around 50 dB and can be rather neglected.

Fiber alignment tolerances along the chip surface have been determined to be around ±7 µm and ±13 µm in orthogonal directions. Further miniaturization of the VCSEL and its monolithic integration in the center of the PD would increase the alignment tolerances as well as the fiber coupling of the VCSEL.

The demonstrated monolithic transceiver design based on a well-established material system is well suited for low-cost and compact optical links over distances of a few hundred meters. Capable to handle data rates of up to 10 Gbit/s, these transceiver chips can be employed, e.g., to upgrade existing standard multimode fiber networks to bidirectional operation.

Acknowledgment

The author thanks D. Wahl for MBE growth of the multilayer structures and S. Paul for previous investigations into VCSEL–PIN PD bidirectional data links. We gratefully acknowledge partial funding of this work by the German Research Foundation (DFG).

References

[1] A. Kern, S. Paul, D. Wahl, A. Al-Samaneh, and R. Michalzik, "Single-fiber bidirectional optical data links with monolithic transceiver chips" (invited), *Advances in Optical Technologies*, Special Issue on *Recent Advances in Semiconductor Surface-Emitting Lasers*, Article ID 729731, 8 pages, 2012, DOI: 10.1155/2012/729731.

[2] A. Kern, S. Paul, D. Wahl, A. Hein, R. Rösch, W. Schwarz, and R. Michalzik, "6 Gbit/s full-duplex multimode fiber link with monolithic VCSEL–PIN transceiver chips", in

Proc. *37th Europ. Conf. on Opt. Commun., ECOC 2011*, paper We.9.LeSaleve.2, three pages. Geneva, Switzerland, Sept. 2011.

[3] A. Kern, A. Al-Samaneh, D. Wahl, and R. Michalzik, "10 Gbit/s bidirectional multimode data link using monolithically integrated VCSEL–PIN transceiver devices", in Proc. *38th Europ. Conf. on Opt. Commun., ECOC 2012*, paper We.1.E.2, three pages. Amsterdam, The Netherlands, Sept. 2012.

[4] K.J. Ebeling, *Integrated Optoelectronics*, Berlin: Springer-Verlag, 1993.

[5] R. Michalzik, A. Kern, M. Stach, F. Rinaldi, and D. Wahl, "True bidirectional optical interconnects over multimode fiber" (invited), in *Optoelectronic Interconnects and Component Integration IX*, A.L. Glebov, R.T. Chen (Eds.), Proc. SPIE 7607, pp. 76070B-1–17, 2010.

[6] A. Kern, D. Wahl, M.T. Haidar, B. Liu, W. Schwarz, R. Rösch, and R. Michalzik, "Monolithic integration of VCSELs and PIN photodiodes for bidirectional data communication over standard multimode fibers", in *Semiconductor Lasers and Laser Dynamics IV*, K.P. Panayotov, M. Sciamanna, A.A. Valle, R. Michalzik (Eds.), Proc. SPIE 7720, pp. 77200B-1–9, 2010.

[7] H.C. Casey Jr., D.D. Sell, and K.W. Wecht, "Concentration dependence of the absorption coefficient for n- and p-type GaAs between 1.3 and 1.6 eV", *J. Appl. Phys.*, vol. 46, no. 1, pp. 250–257, 1975.